

Two implementations of the Projector Augmented Wave (PAW) formalism

Marc Torrent^a, N. A. W. Holzwarth^b, François Jollet^a, David Harris^b, Nicholas Lepley^b, and Xiao Xu^b

^aCEA, DAM, DIF F-91297 Arpajon, France; ^bDepartment of Physics, Wake Forest University, Winston-Salem, NC, USA

Introduction

The tools available for detailed first-principles studies of materials have benefited enormously from the development of several international collaborations engaged in developing open source electronic structure code packages. These collaborations have resulted in well-designed shared codes which incorporate many of the best “state of the art” methodologies. Validation is an important aspect of code development and most of the collaboration teams have incorporated internal tests as part of their development procedures. The availability of several independently developed codes, provides the opportunity for further testing and validation.

The present poster deals with the identification and analysis of a particular discrepancy between two independent codes in their implementation the projector augmented wave (PAW) method developed by Blöchl.¹ We show that the discrepancy can be traced to a slight formalism difference in the two implementations. Since one of the codes (ABINIT)² is widely used and because our analysis may be relevant to some of the other codes which have adopted the PAW method, we thought it useful to present our findings.

Calculational Methods

All calculations were performed within the framework of density functional theory³ using exchange correlation functionals with either the local density approximation (LDA),⁴ or the generalized gradient approximation (GGA).⁵ The independent codes used for the comparison of PAW implementations are PWPAW⁶ and ABINIT² using the same PAW basis and projector functions generated using the ATOMPAW code⁷ and the *atompaw2abinit* converter program available at the ABINIT website.

These codes have been compared with each other and with other independent codes, and for most materials the agreement is excellent. However, three example materials serve to illustrate the discrepancy. These materials use the PAW basis and projector function parameters listed in Table I.

TABLE I PAW parameters used in calculations: the pseudopotential radius r_c^a (in bohr), list of shell designations $n_1l_1(r_{m_1})n_2l_2(r_{m_2})\dots$ of basis and projector functions used in the calculation and corresponding radii r_{m_i} (in bohr) used to match the all-electron and pseudo radial wavefunctions. The symbol ϵ indicates the use of unbound basis functions with energies $\epsilon = 2.0, 0.0,$ and 3.0 Ry for F, Si, and Cu, respectively.

Atom	r_c^a	$\{n_i l_i(r_{m_i})\}$
Li	1.7	1s(1.4) 2s(1.7) 2p(1.7)
F	1.5	2s(1.5) ϵ s(1.5) 2p(1.5) ϵ p(1.5)
Si (valence)	2.0	3s(2.0) 3p(2.0) ϵ d(2.0)
Si (semicore)	1.5	2s(1.5) 3s(1.5) 2p(1.5) 3p(1.5)
Cu	2.3	3s(1.5) 4s(2.2) 3p(1.5) 4p(2.2) 3d(1.5) ϵ d(2.2)

The first example is the highly ionic material LiF in the rock-salt structure. Figure 1 shows plots of electronic energy versus cubic lattice parameter a , comparing the PAW results from both PAW codes with the all-electron results generated by the WIEN2k code.⁸ In general there is excellent agreement among all of the results, with the obvious exception of the ABINIT results for the GGA functional, where the equilibrium lattice constant is found to be 0.006 nm larger than that of the others.

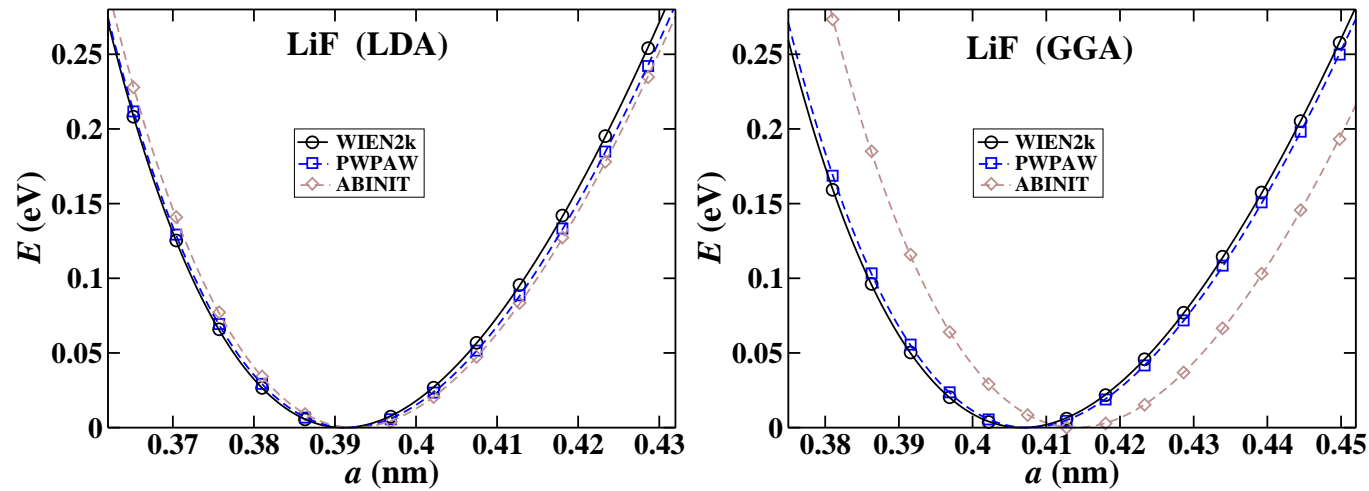


FIG. 1 Plots of electronic energy (E) of LiF as a function of lattice constant (a) determined from the WIEN2k, PWPAW, and ABINIT codes, comparing LDA (left plot) and GGA (right plot) results.

The second example is Si in the diamond structure is shown in Fig. 2. In this case, only the GGA results are presented for two different basis and projector sets – “valence” and “semicore” defined in Table I. We see that while the “valence” basis set gives results in good agreement between WIEN2k, PWPAW, and ABINIT, the “semicore” basis set used with the ABINIT code results in a discrepancy compared the other results. While this discrepancy is not as large as the discrepancy for the GGA functional results of LiF, it is larger than it should be if the codes were performing the same calculations with the same input parameters, as designed.

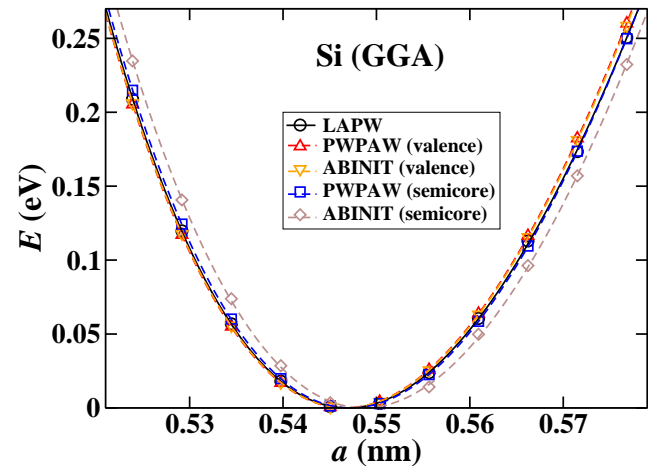


FIG. 2 Plot of the electronic energy (E) of Si as a function of lattice constant (a) calculated using the GGA functional, comparing results using 3 codes and 2 different PAW basis and projector sets as explained in Table I and in the text.

The third example of Cu will be shown later. These three examples show extreme examples of the discrepancies between the two codes. By contrast, there are many other materials which show excellent agreement between the two codes. As we will show, the origin of the discrepancies turns out to be due to a subtle difference in formalisms.

The basic idea developed by Blöchl¹ can be summarized in terms of the PAW expression of the valence electron energy of the system as a combination of smooth contributions evaluated over all space plus a sum of atom-centered terms which contribute within “augmentation” spheres, of radii r_c^a about each atomic site a :

$$E_{\text{vale}} = \underbrace{\tilde{E}_{\text{vale}}}_{\text{pseudo-energy}} + \sum_a \underbrace{\left(E_{\text{vale}}^a - \tilde{E}_{\text{vale}}^a \right)}_{\text{atom-centered corrections}}. \quad (1)$$

In principle, the pseudo-energy contributions within each augmentation sphere are canceled out of the expression by the atom-centered pseudo-energy $\tilde{E}_{\text{vale}}^a$ and replaced by the atom-centered full nodal valence energy E_{vale}^a . Provided that the cancellation is well approximated, there is considerable freedom in the formulation of pseudofunctions within the augmentation spheres. Consequently, there are some variations in the detailed formulations of the PAW method described in the literature. The ABINIT formulation⁹ follows that of Kresse¹⁰ which, apart from regrouping of the terms in the expressions, differs from the original formulation of Blöchl in the treatment of the pseudo exchange-correlation contributions. In particular, denoting by $n(\mathbf{r})$ and $n_c(\mathbf{r})$ the valence and core electron fully nodal charge densities and by $\tilde{n}(\mathbf{r})$ and $\tilde{n}_c(\mathbf{r})$ the corresponding valence and core electron pseudo-densities, Blöchl’s form of the exchange-correlation energies can be expressed in terms of the functional dependencies:

$$E_{xc}^B = E_{xc}[\tilde{n} + \tilde{n}_c] + \sum_a \left(E_{xc}^a[n^a + n_c^a] - E_{xc}^a[\tilde{n}^a + \tilde{n}_c^a] \right). \quad (2)$$

Including the smooth core pseudo-densities in the evaluation of the functional follows the notion of the non-linear core correction introduced by Louie *et. al*¹¹ which has been demonstrated to work well for norm-conserving pseudopotentials and also works well for the PAW formalism. On the other hand Kresse’s version of the exchange-correlation energies has the form

$$E_{xc}^K = E_{xc}[\tilde{n} + \tilde{n}_c + \hat{n}] + \sum_a \left(E_{xc}^a[n^a + n_c^a] - E_{xc}^a[\tilde{n}^a + \tilde{n}_c^a + \hat{n}^a] \right). \quad (3)$$

Here the extra term $\hat{n}(\mathbf{r})$ is the valence compensation charge, which can be defined in the notation of references [10] and [9] to be

$$\hat{n}(\mathbf{r}) = \sum_{aijLM} \rho_{ij}^a \hat{Q}_{ij}^{aLM}(\mathbf{r}), \quad (4)$$

where a is the atomic site index, ij are basis and projector function indices and LM are spherical harmonic indices.

The coefficients ρ_{ij}^a are determined from the Bloch pseudowavefunctions $\tilde{\Psi}_{n\mathbf{k}}(\mathbf{r})$ and the projector functions $\tilde{p}_i^a(\mathbf{r})$ by the expression

$$\rho_{ij}^a = \sum_{n\mathbf{k}} f_{n\mathbf{k}} \langle \tilde{\Psi}_{n\mathbf{k}} | \tilde{p}_i^a \rangle \langle \tilde{p}_j^a | \tilde{\Psi}_{n\mathbf{k}} \rangle, \quad (1)$$

where $f_{n\mathbf{k}}$ represents the sampling weight and occupancy of the Bloch state. The compensation spatial functions $\hat{Q}_{ij}^{aLM}(\mathbf{r})$ are localized within the augmentation sphere of atom a and have the form

$$\hat{Q}_{ij}^{aLM}(\mathbf{r}) \equiv q_{ij}^{LM} g_L(|\mathbf{r} - \mathbf{R}^a|) Y_{LM}(\widehat{\mathbf{r} - \mathbf{R}^a}), \quad (2)$$

where $Y_{LM}(\widehat{\mathbf{r} - \mathbf{R}^a})$ denotes a spherical harmonic function, q_{ij}^{LM} is a coefficient representing the LM^{th} moment associated with the pair of basis functions i and j , and $g_L(|\mathbf{r} - \mathbf{R}^a|)$ denotes a radial shape function with the properties

$$g_L(r) \equiv 0 \quad \text{for } r \geq r_c^a \quad \text{and} \quad \int_0^{r_c^a} dr r^{2+L} g_L(r) = 1. \quad (3)$$

The purpose of the compensation charge density $\hat{n}(\mathbf{r})$ is to add the correct amount of charge moments to the valence pseudo-density

$$\tilde{n}(\mathbf{r}) \equiv \sum_{n\mathbf{k}} f_{n\mathbf{k}} |\tilde{\Psi}_{n\mathbf{k}}(\mathbf{r})|^2 \quad (4)$$

so that outside the augmentation region of all the atoms, the Coulomb (or Hartree) potential for the sum of the valence pseudo and compensation charge densities $\tilde{n}(\mathbf{r}) + \hat{n}(\mathbf{r})$ is the same as that for the fully nodal valence electron density $n(\mathbf{r})$:

$$V_H(\mathbf{r}) = \int d^3r' \frac{\tilde{n}(\mathbf{r}') + \hat{n}(\mathbf{r}')}{|\mathbf{r} - \mathbf{r}'|} \Big|_{|\mathbf{r} - \mathbf{R}^a| > r_c^a} \int d^3r' \frac{n(\mathbf{r}')}{|\mathbf{r} - \mathbf{r}'|}. \quad (5)$$

While the inclusion of compensation charge density $\hat{n}(\mathbf{r})$ is essential to correctly represent the Coulombic interactions of the system, it is not obvious that $\hat{n}(\mathbf{r})$ has any physical meaning in the argument of exchange-correlation functionals which are based on either a local density approximation (LDA) or a generalized gradient approximation (GGA). For these functionals, at any given spatial point \mathbf{r} , the exchange-correlation contribution depends on the density (and its gradient in the case of GGA) at that point. Formally, all pseudofunction contributions within the augmentation sphere, cancel out of the energy and Hamiltonian expressions, so that in general, the presence of the compensation charge in the exchange-correlation functional the expression should do no harm. However, in some cases, such as those presented in the introduction, inclusion of $\hat{n}(\mathbf{r})$ in the argument of the pseudo exchange-correlation functional can introduce non-canceling errors as will be demonstrated in more detail in below.

Examples

In most of our calculations, the squared sinc function was used for the compensation charge shape:

$$g_L(r) = \begin{cases} \mathcal{N}_L r^L \left(\frac{\sin(\pi r/r_c^a)}{\pi r/r_c^a} \right)^2 & \text{for } r \leq r_c^a \\ 0 & \text{for } r > r_c^a \end{cases}, \quad (6)$$

where \mathcal{N}_L is a normalization constant. We also considered the use of a Bessel function shape of the form:¹⁰

$$g_L^B(r) = \begin{cases} \mathcal{N}_L \left[j_L \left(\frac{x_{L1} r}{r_{comp}} \right) - \frac{x_{L1} j_L'(x_{L1})}{x_{L2} j_L'(x_{L2})} j_L \left(\frac{x_{L2} r}{r_{comp}} \right) \right] & \text{for } r \leq r_{comp} \\ 0 & \text{for } r > r_{comp} \end{cases}, \quad (7)$$

where x_{Li} denotes the i^{th} zero of the spherical Bessel function $j_L(x)$ and \mathcal{N}_L denotes a normalization constant. Kresse *et al.* recommend that the radius parameter be chosen such that $r_c^a/r_{comp} \approx 1.2$.

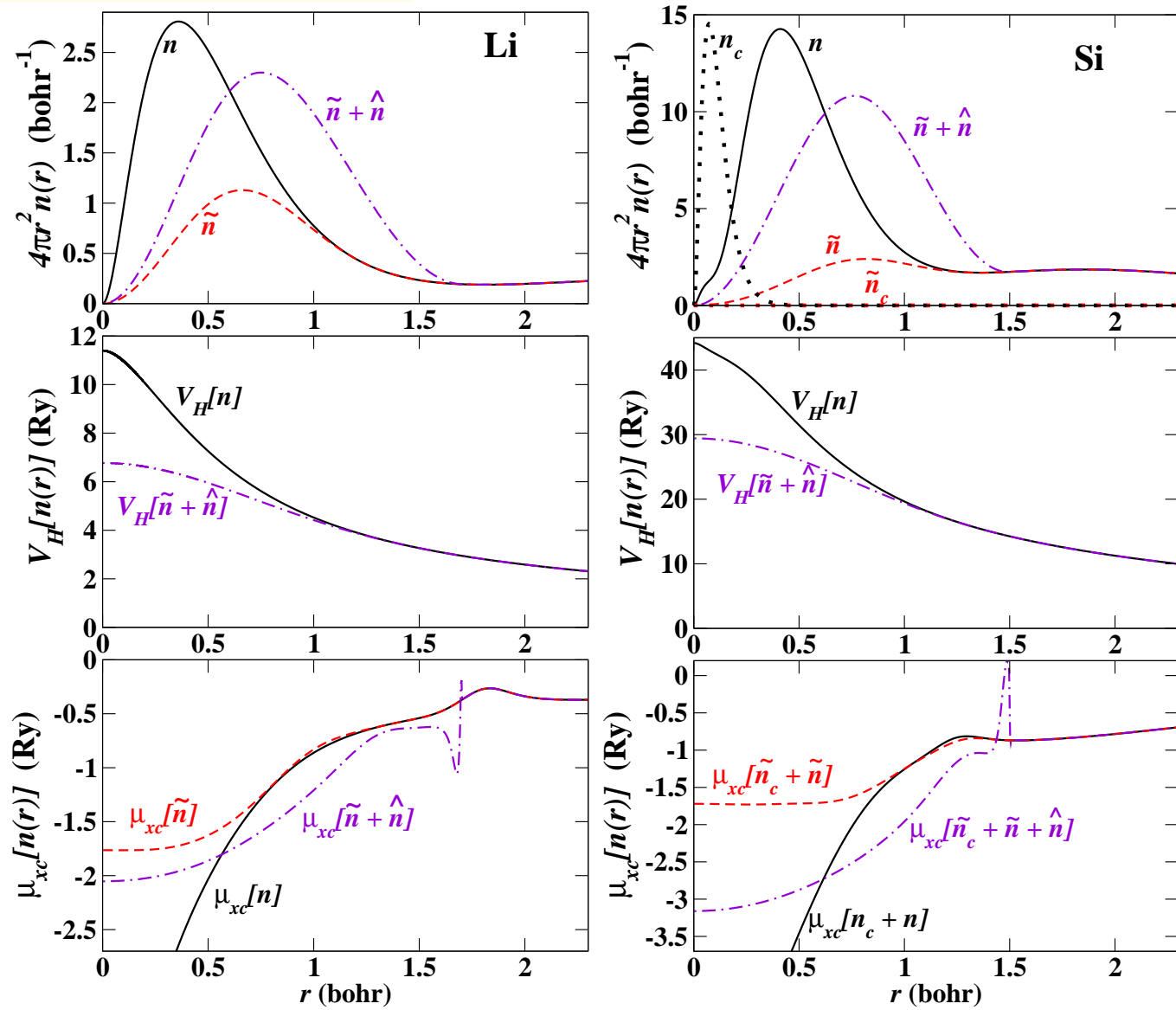


FIG.3

Plots of radial charge densities (top panel), Hartree potentials (second panel), and GGA exchange-correlation potentials (lower panel) for Li (left) and Si (right). In both cases, semi-core states were included in the basis configuration and the compensation charge density \hat{n} is constructed using the squared sinc function defined in Eq. (6).

In both of the examples shown in Fig. 3, we see that the compensation charge density causes the Hartree pseudo-potential $V_H[\tilde{n} + \hat{n}]$ to converge smoothly to Hartree full potential $V_H[n]$ as $r \rightarrow r_c^a$. On the other hand, for the exchange-correlation pseudo-potential in the Kresse formulation, $\mu_{xc}[\tilde{n}_c + \tilde{n} + \hat{n}]$ shows unphysical behavior near $r \leq r_c^a$ due to a significant discontinuity in the curvature of $[\tilde{n}_c + \tilde{n} + \hat{n}]$ in that region while in the Blöchl formulation, $\mu_{xc}[\tilde{n}_c + \tilde{n}]$ is well behaved and converges smoothly to the full potential $\mu_{xc}[n_c + n]$ as $r \rightarrow r_c^a$.

FIG. 4 GGA exchange-correlation potentials for Cu using $r_c^a = 2.3$ bohr, comparing functionals of all-electron density ($n_c + n$), Blöchl's pseudodensity ($\tilde{n}_c + \tilde{n}$), and Kresse's pseudodensity ($\tilde{n}_c + \tilde{n} + \hat{n}$) using the squared sinc compensation charge shape, and ($\tilde{n}_c + \tilde{n} + \hat{n}^B$) using the Bessel function compensation charge shape.

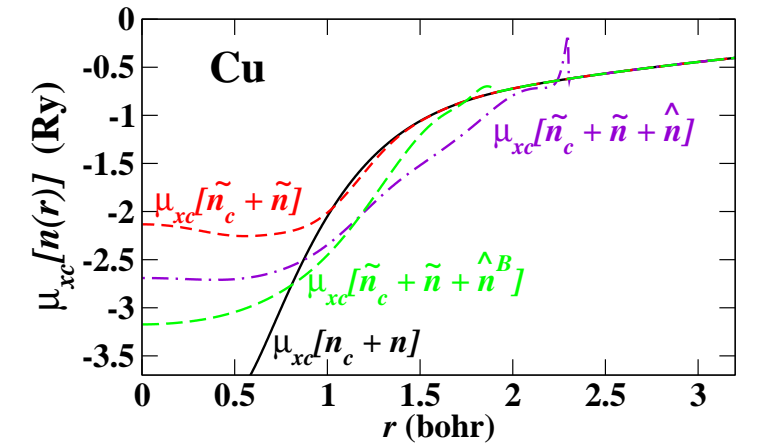


Figure 4 compares the GGA exchange-correlation functionals of Cu constructed using Blöchl's form and Kresse's form with two different compensation charge shapes both generated using the ATOMPAW code. In this example, we see that for using the Kresse form of the exchange-correlation treatment, the Bessel shape function for the compensation charge is numerically much better behaved than is the squared sinc function. However, it is again clear that the Blöchl form of the exchange-correlation treatment (using $\mu_{xc}[\tilde{n}_c + \tilde{n}]$) converges most smoothly to the all-electron function in the neighborhood of the augmentation sphere boundary.

These examples of discontinuous behavior of pseudo exchange-correlation potentials are obviously extreme cases, chosen to illustrate the problem clearly. In the examples shown in Figs. 2-4, it is apparent that the discontinuities in the pseudo exchange-correlation potentials near r_c^a seem to be the likely cause of the discrepant structural results presented here.

In order to verify our analysis of this problem we have written modified versions of the ATOMPAW, ABINIT, and PWPAW codes, allowing for the treatment of both the Blöchl and Kresse formulations of exchange-correlation energies (Eqs. 6 and 7) and the corresponding Hamiltonian terms within each of the codes. Figure 5 shows the results for Cu using the exchange-correlation functional, comparing the both the Blöchl and Kresse forms using both of the modified codes.

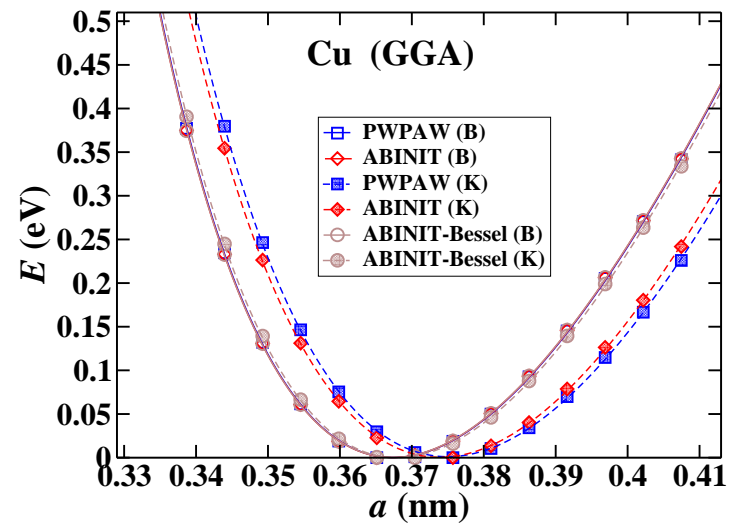


FIG. 5 Comparison of binding energy curves for Cu using the GGA exchange-correlation functional using the Blöchl (B) and Kresse (K) formalisms and the modified PWPAW and ABINIT codes. Also shown are results using the Bessel compensation charge shape (Eq. 7) in both schemes using the ABINIT code.

Here we see that all results using the Blöchl formalism are in excellent numerical agreement. The results from the two codes using the Kresse form with the squared sinc function have a relatively small numerical discrepancy with each other, undoubtedly due to slightly different treatments of the discontinuous exchange-correlation functional. The ABINIT code is also able to use the Bessel shape compensation charge (Eq. (7)) and those results are also shown in Fig. 5. In this case, both the Kresse and Blöchl forms are in good agreement with each other and with the results of the Blöchl form using the squared sinc function.

Table II summarizes the numerical results of all of the test cases considered in this study. From this table and from the binding energy curves given in Fig. 1, 2, and 5, it is clear that the original Blöchl PAW formalism for the exchange-correlation contributions (2) avoids numerical difficulties that can occur with the Kresse formulation (3). In order to clarify the issue, we have chosen extreme examples of the problem. From these examples, it is apparent that the origin of the problem is due to the fact that the exchange-correlation functions are very sensitive to the local shape of the density. Since these functionals were designed^{5,6} to represent physical densities it is perhaps not surprising that the arbitrary shape of the valence compensation charge can cause spurious exchange-correlation contributions particularly when it is significantly larger than the physical density.

TABLE II Ground state parameters for LiF, Si, and Cu determined from fit of calculations to the Murnaghan¹² equation of state, listing the equilibrium lattice constant a_0 (nm) and bulk modulus B (GPa). The notation (B) and (K) denote the Blöchl and Kresse formalisms respectively. For Si, (v) and (s) denote the valence and semicore basis sets respectively. Two calculations for Cu were performed using the Bessel function compensation charge shape (Eq. 7) with the notation [Bes]; otherwise, the squared sinc shape (Eq. 6) was used.

Method	LDA		GGA	
	a_0	B	a_0	B
LiF				
WIEN2k	0.391	87	0.407	66
PWPAW (B)	0.392	85	0.408	66
ABINIT (K)	0.392	85	0.414	66
Si				
WIEN2k			0.547	87
PWPAW (B) (v)			0.547	89
ABINIT (K) (v)			0.547	88
PWPAW (B) (s)			0.547	88
ABINIT (K) (s)			0.549	87
Cu				
WIEN2k	0.355	170	0.366	130
PWPAW (B)	0.356	160	0.367	120
ABINIT (B)	0.356	160	0.367	120
ABINIT (B) [Bes]			0.367	120
ABINIT (K) [Bes]			0.368	120
PWPAW (K)			0.375	110
ABINIT (K)	0.357	160	0.374	110

We expect that this problem will become even more serious as more complicated functionals are developed which can depend on higher order density derivatives.¹³

In practice, the error we have identified can be ameliorated by choosing other radial shape functions than the squared sinc function defined in Eq. (6). The example for Cu using the Bessel function shape compensation charge defined in Eq. (7) illustrates this effect quite well.

Summary and Conclusions

As a result of this analysis, we conclude that the Blöchl formulation of the exchange-correlation terms of the PAW method provides the best numerical stability. In principle, using the compensation charge contributions only for the Coulombic contributions for which they were designed, allows for greater choice in the shape functions which can give both physical results and optimized plane wave convergence parameters. Furthermore, the numerical evaluation of the exchange-correlation terms can be done more efficiently in the Blöchl formulation compared to the Kresse formulation since the evaluation of \hat{n} within the exchange-correlation calculations is relatively time-consuming. A new version of ABINIT has been prepared and will be available in production release 6.1 and higher which has the option of using the Blöchl exchange-correlation formulation.

While we have argued that the Kresse formulation of the exchange-correlation terms of the PAW method is poorly motivated and can lead to numerical difficulties, we would like to stress that the problems we have identified affect a relatively small number of calculations. With careful control of the parameters, both the Blöchl and Kresse formulations of the PAW method can produce results consistent with all-electron results. The experiences learned in this analysis reinforces the fact that the quantitative accuracy of PAW and other pseudopotential methods relies on careful scrutiny and testing of the pseudopotential parameters used in the calculations. The ABINIT website (<http://www.abinit.org>) gives the following excellent advice: “Pseudopotentials should always be tested in well-known situations, before using them for predictions.”

Acknowledgements

We would like to acknowledge Bernard Amadon for fruitful discussions. The portion of this work performed at Wake Forest University was supported by NSF grants NSF DMR-0405456, DMR-0427055, and DMR-0705239 with computations performed on the Wake Forest University DEAC cluster, a centrally managed resource with support provided in part by the University. David Harris contributed to the database of PAW projector and basis functions available on the website <http://www.wfu.edu/~natalie/papers/pwpaw/periodictable/periodictable.html> over several summers while enrolled as a physics student at the University of North Carolina at Chapel Hill. WFU graduate students Nicholas Lepley and Xiao Xu also contributed to the database. Earlier work by summer students John Tumbleston and Nicholas Dellaripa is also acknowledged.

Bibliography

- [1] P. E. Blöchl, *Phys. Rev. B* **50**, 17953 (1994)
- [2] X. Gonze, B. Amadon, P. M. Anglade, *et. al*, *Comput. Phys. Commun.* **180**, 2582 (2009); Code is available at the website <http://www.abinit.org>.
- [3] P. Hohenberg and W. Kohn. *Phys. Rev.* **136** B864, (1964); W. Kohn and L. J. Sham, *Phys. Rev.* **140** A1133, (1965).
- [4] J. P. Perdew and Y. Wang, *Phys. Rev. B* **45**, 13244 (1992).
- [5] J. P. Perdew, K. Burke, M. Ernzerhof, *Phys. Rev. Lett.* **77** 3865 (1996); **78** 1396 (1997).
- [6] A. R. Tackett, N. A. W. Holzwarth, and G. E. Matthews, *Comput. Phys. Commun.* **135**, 348 (2001).
- [7] N. A. W. Holzwarth, A. R. Tackett, and G. E. Matthews, *Comput. Phys. Commun.* **135**, 329 (2001); Code is available at the website <http://pwpaw.wfu.edu>.
- [8] P. Blaha, K. Schwarz. G. Madsen, D. Kvasnicka, and J. Luitz, Techn. Universität Wien, Austria (2001), www.wien2k.at.
- [9] M. Torrent, F. Jollet, F. Bottin, G. Zérah, and X. Gonze, *Comput. Materials Science* **42** 337 (2008).
- [10] G. Kresse and D. Joubert, *Phys. Rev. B* **59** 1758 (1999).
- [11] S. G. Louie, S. Froyen, and M. L. Cohen, *Phys. Rev. B* **26** 1738 (1982).
- [12] F. D. Murnaghan, *Proc. Nat. Acad. Sci. USA* **30** 244 (1944).
- [13] J. P. Perdew, A. Ruzsinszky, G. I. Csonka, L. A. Constantin, and J. Sun, *Phys. Rev. Lett.* **103** 026403 (2009).